Imaging Science in Dentistry 2018; 48: 245-54
https://doi.org/10.5624/isd.2018.48.4.245

Effect of object position in the field of view and application of a metal artifact reduction algorithm on the detection of vertical root fractures on cone-beam computed tomography scans: An *in vitro* study

Ava Nikbin[1], Zahra Dalili Kajan[2,*], Mehran Taramsari[3], Negar Khosravifard[2]

[1]*Department of Maxillofacial Radiology, Faculty of Dentistry, Guilan University of Medical Sciences, Rasht, Iran*
[2]*Dental Sciences Research Center, Department of Maxillofacial Radiology, Faculty of Dentistry, Guilan University of Medical Sciences, Rasht, Iran*
[3]*Dental Sciences Research Center, Department of Endodontics, Faculty of Dentistry, Guilan University of Medical Sciences, Rasht, Iran*

ABSTRACT

Purpose: To assess the effects of object position in the field of view (FOV) and application of a metal artifact reduction (MAR) algorithm on the diagnostic accuracy of cone-beam computed tomography (CBCT) for the detection of vertical root fractures (VRFs).

Materials and Methods: Sixty human single-canal premolars received root canal treatment. VRFs were induced in 30 endodontically treated teeth. The teeth were then divided into 4 groups, with 2 groups receiving metal posts and the remaining 2 only having an empty post space. The roots from different groups were mounted in a phantom made of cow rib bone, and CBCT scans were obtained for the 4 different groups. Three observers evaluated the images independently.

Results: The highest frequency of correct diagnoses of VRFs was obtained with the object positioned centrally in the FOV, using the MAR algorithm. Peripheral positioning of the object without the MAR algorithm yielded the highest sensitivity for the first observer (66.7%). For the second and third observers, a central position improved sensitivity, with or without the MAR algorithm. In the presence of metal posts, central positioning of the object in the FOV significantly increased the diagnostic sensitivity and accuracy compared to peripheral positioning.

Conclusion: Diagnostic accuracy was higher with central positioning than with peripheral positioning, irrespective of whether the MAR algorithm was applied. However, the effect of the MAR algorithm was more significant with central positioning than with peripheral positioning of the object in the FOV. The clinical experience and expertise of the observers may serve as a confounder in this respect. ***(Imaging Sci Dent 2018; 48: 245-54)***

KEY WORDS: Tooth Fracture; Artifact; Diagnosis; Cone-Beam Computed Tomography

Introduction

Vertical root fractures (VRFs) may occur during or after root canal treatment or following the insertion of screws, retentive pins and intracanal posts.[1] VRF is the most severe type of longitudinal fracture, and usually initiates from the apical part of the root and propagates towards the coronal part.[2] Alternatively, depending on the stressors, VRFs may initiate from the cervical region.

Considering the acknowledged limitations of intraoral radiography, the poor or even hopeless prognosis of VRFs, and the need to extract such teeth, a more efficient and reliable imaging modality is required to promote the accurate detection of VRFs in order to prevent the extra costs imposed on patients for futile attempts made by dental clinicians to save such teeth. The inability of conventional radiography to visualize VRFs highlights the need for a more advanced diagnostic imaging modality, such as cone-beam

*This research was supported financially by Vice-Chancellor in Research Affairs, Guilan University of Medical Sciences.
Received June 15, 2018; Revised August 14, 2018; Accepted August 24, 2018
*Correspondence to : Prof. Zahra Dalili Kajan
Department of Maxillofacial Radiology, Dental School, The End of Professor Samii Blvd. Rasht, Iran
Tel) 98-131-3263622, Fax) 98-131-3263621, E-mail) zahradalili@yahoo.com

Imaging Science in Dentistry · pISSN 2233-7822 eISSN 2233-7830

computed tomography (CBCT), for this purpose.[3]

CBCT scanners are available with different fields of view (FOVs). The volume of the FOV has a direct correlation with the exposure/radiation dose. Accurate geometry and multiplanar reconstruction are among the main advantages of CBCT compared to conventional radiography. Image reconstruction in the sagittal, coronal, and axial planes in CBCT eliminates the superimposition of anatomical structures.[4] However, CBCT also has shortcomings. The quality of reconstructed CBCT images is affected by noise, beam hardening, the cone-beam effect, and photon starvation. These effects result in the formation of various types of artifacts, such as bright streaks of radiation, dark areas adjacent to metal objects, or even the complete loss of gray shadows between adjacent metal objects. Consequently, the region of interest for treatment planning may not be clearly visualized.[5,6]

Several studies have evaluated the application of CBCT for detecting VRFs,[7-12] and all have confirmed the superiority of CBCT to conventional radiography for this purpose, despite the fact that metal artifacts pose an impediment to the diagnostic quality of CBCT. Metal artifacts, with their negative impact on accuracy, can affect treatment planning and are therefore the main problem of CBCT.

As theorized using mathematical modeling, beam hardening adjacent to metal objects is due to the different X-ray absorption coefficients of bone and metal objects. Accordingly, some CBCT systems have been equipped with a metal artifact reduction (MAR) algorithm, which employs several techniques for image reconstruction, including pre-processing and post-processing algorithms. In the pre-processing algorithm, the metal object is located in the basic projection data and then the metal projection data are processed using an interpolation algorithm. Eventually, axial images are reconstructed using pre-processed adjustments in the basic data and the metal part is modified and retrieved. The post-processing algorithm is based on segmentation and modification of the metal part in each exposure, and the final CT image is reconstructed using the modified data. It appears that the pre-processing algorithm is more effective at improving image quality in areas adjacent to metal objects.[13]

Some studies have evaluated the effects of FOV size and object position in the FOV on noise reduction,[14,15] as well as the effects of artifact reduction[16,17] on the quality of CBCT images. Queiroz et al.[15] evaluated the effect of object position in the FOV and the MAR algorithm on noise reduction and reported lower levels of noise for objects positioned at the center of the FOV than for objects at the periphery. Moreover, a significant reduction in the level of noise was noted following the activation of the MAR tool when the object was at the center of the FOV. Therefore, this study aimed to assess the effects of object position in the FOV and application of the MAR algorithm on the diagnostic accuracy of CBCT images for the detection of VRFs.

Materials and Methods

This *in vitro* experimental study was conducted on 60 human single-canal premolars that had been extracted for orthodontic purposes. The ethical approval code for this study was IR.GUMS.REC.1396.241. The selected teeth had no root caries, root fractures, or severe root curvature. Teeth with severe root curvature upon clinical observation were excluded. The external root surface was debrided of tissue residue and debris, and the teeth were immersed in 5.25% sodium hypochlorite solution for 24 hours. The teeth were decoronated at the cementoenamel junction using a diamond disc and underwent root canal therapy with the same technique. After 24 hours, the post space was prepared using #2 and #3 Peeso reamers to half of the working length. To simulate the periodontal ligament space, a layer of green wax was applied on the root surface.

Two pieces of cow rib bone with adequate thickness were fixed to both ends of a wax arch to simulate part of the mandibular body. Cavities simulating extraction sockets were created in it, and the tooth roots were placed in them and fixed in position (Fig. 1). Alveolar sockets were cre-

Fig. 1. A photograph showing the phantom fabricated for the placement of teeth after tooth insertion.

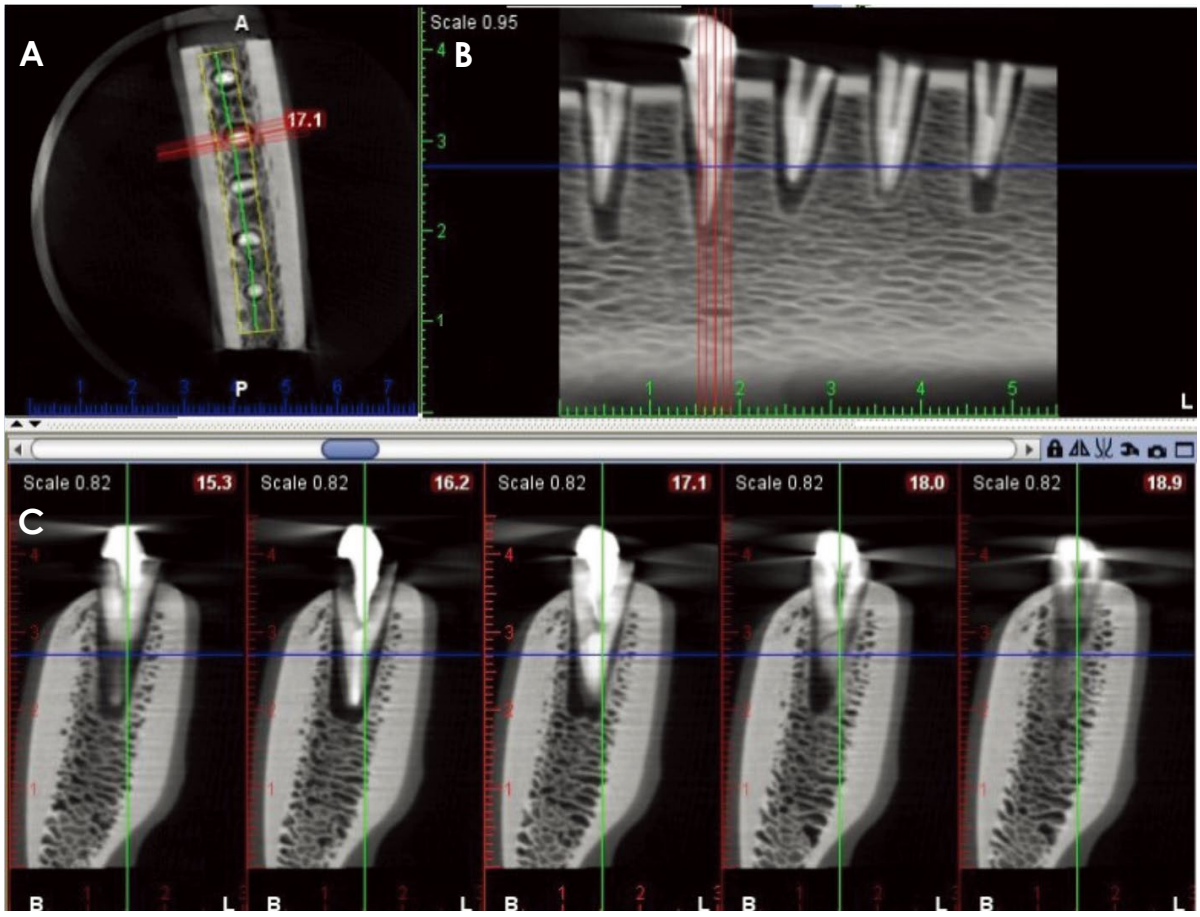

Fig. 2. Cone-beam computed tomographic images with central positioning of the object in the field of view. An axial image (A) and cross-sectional images (B and C) reveal root fracture of the left second tooth.

ated by a bur. In prepared sockets that were larger than the teeth, the excess space was filled with wax.

In 30 of the 60 endodontically treated teeth, a fracture was induced without displacement. For fracture induction, an intracanal pin larger than the post space was inserted into the root and screwed by a screwdriver to cause a fracture. The authors tried their best to induce small root fractures without displacing the broken segments. The presence of a root fracture was confirmed by visual observation of the fracture line. All fractures were longitudinal, vertical, and oblique.

The teeth were divided into 4 groups of 15. In group 1, the teeth had VRFs, and intracanal casting posts were fabricated and cemented into the roots. In group 2, the teeth had VRFs, and the post space remained empty. In group 3, the teeth did not have VRFs, and casting posts were cemented into the roots. In group 4, the teeth did not have VRFs, and the post space remained empty.

The teeth were randomly mounted in the fabricated arch and radiographed. Teeth from the 4 groups were mounted in the arch in a completely random order, and the observers were blinded to the group allocation of the teeth mounted in the arch.

The phantom was placed in a cylindrical U-shaped model containing water for soft tissue reconstruction and then placed on the chin rest of a CBCT system (Planmeca, Helsinki, Finland) such that the occlusal plane was parallel to the ground. Next, the 3-dimensional (3D) program was chosen and the mandible was radiographed once with a central target and the selection of "half" (50 mm height and 80 mm diameter of FOV) in the FOV menu. The exposure rate was automatically determined by the system. The MAR algorithm was not enabled (first mode). In the second mode, each of the right and left sides were radiographed by choosing "molar" (50 mm height and 80 mm diameter of FOV) in the target feature interface, without enabling the MAR algorithm.

In the first mode, the source generating the metal artifact (including the intracanal post and gutta-percha) was located peripherally in the FOV. In the second mode, the

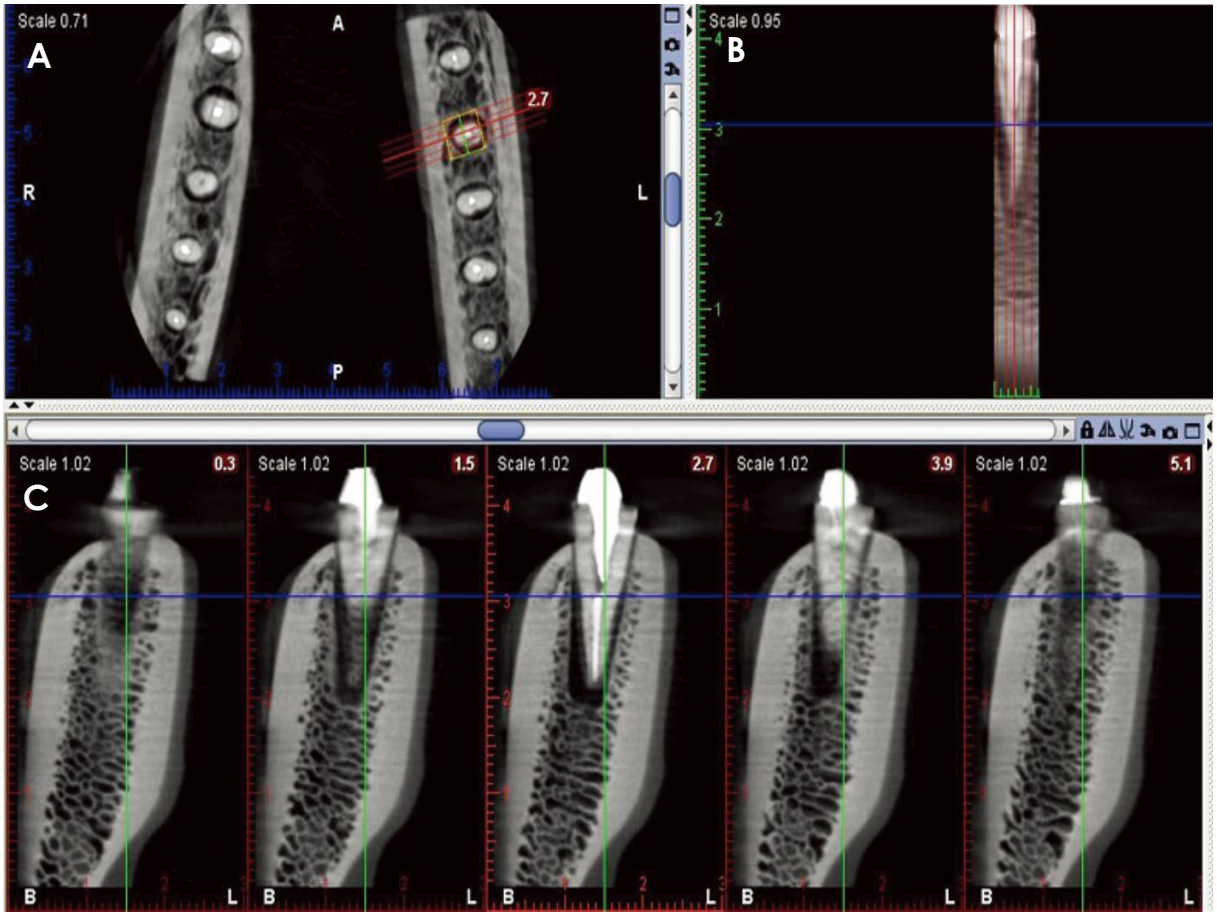

Fig. 3. Cone-beam computed tomographic images with peripheral positioning of the object in the field of view. An axial image (A) and cross-sectional images (B and C) reveal root fracture of the left second tooth.

source generating the metal artifact was positioned centrally in the FOV. In both modes, high resolution (0.16 mm voxel size) was selected before exposure. In the first mode, the *x* and *z* coordinates of imaging were 0 and 37, respectively. These coordinates in the second mode were –30 and 33 for the right side and 25 and 41 for the left side, respectively. These conditions remained the same throughout the entire imaging process. The third mode and fourth modes were similar to the first and second modes, respectively, but the MAR algorithm was enabled during imaging.

The images were stored using Romexis Viewer version 5.2 (Planmeca, Helsinki, Finland) and 3 observers, including 2 oral and maxillofacial radiologists and 1 endodontist, observed the images. The endodontist (observer 3) and one of the maxillofacial radiologists (observer 1) had more than 15 years of experience, while the second maxillofacial radiologist (observer 2) had 6 years of experience and was trained and calibrated. All 3 observers were involved in diagnosing root fractures as part of their clinical responsibilities. The observers were free to use reconstructed axial and cross-sectional images and to change the density or contrast of the radiographs. The observers mainly used slice thicknesses of 0.5-1.5 mm, which they could change during observation. Figures 2 and 3 show root fractures with peripheral and central positioning of objects that were visualized with the MAR algorithm. The observers were requested to report the presence of VRFs using the following scoring system:[7] 1, VRF definitely absent; 2, VRF probably absent; 3, VRF probably present; 4, VRF definitely present.

Inter-observer agreement was calculated using kappa statistics. The data were analyzed using SPSS version 22 (IBM Corporation, Armonk, NY, USA) and STATA version 12 (Stata Corporation, Texas, USA). The sensitivity, specificity, accuracy, positive predictive value (PPV), negative predictive value (NPV), positive likelihood ratio (LR+) and negative likelihood ratio (LR–) were calculated for each imaging mode and in the 2 groups of teeth with intracanal posts and teeth with empty post space.

Table 1. Comparison of the frequency of correct diagnoses of vertical root fractures by the 3 observers on cone-beam computed tomographic scans taken with different modes according to the position of the object in the field of view and application of the metal artifact reduction (MAR) algorithm

	Peripheral + no MAR	Peripheral + MAR	Central + no MAR	Central + MAR	*P* value
Observer 1	20 (66%)	16 (53%)	19 (63%)	19 (63%)	0.92
Observer 2	7 (23%)	14 (47%)	15 (50%)	19 (63%)	$P<0.01$
Observer 3	16 (53%)	16 (53%)	18 (60%)	18 (60%)	0.97

Table 2. Inter-observer agreement among the 3 observers using kappa statistics

Observers' agreement	Peripheral + no MAR	Peripheral + MAR	Central + no MAR	Central + MAR
Observers 1, 2, and 3	0.18	0.50	0.43	0.59

MAR: metal artifact reduction

Results

In this *in vitro* experimental study, 60 single-canal premolars (30 with VRFs and 30 without VRFs, 15 in each group defined by the presence or absence of metal casting posts) were used to assess the effects of tooth position in the FOV and application of the MAR algorithm on the detection of VRFs on CBCT images.

The frequency of correct diagnoses of VRF in the 4 different modes, including peripheral positioning of the object in the FOV with and without activating the MAR algorithm and central positioning of the object in the FOV with and without activating the MAR algorithm, was evaluated for the 3 observers. The results are presented in Table 1.

The first observer had the highest frequency of correct diagnoses of VRF for objects positioned peripherally in the FOV without use of the MAR algorithm. The second observer had the highest frequency of correct diagnoses of VRF for objects positioned centrally in the FOV with the MAR algorithm applied. The third observer had the highest frequency of correct diagnoses of VRF for objects centrally positioned in the FOV with or without applying the MAR algorithm. This difference was only significant for the second observer ($P<.01$).

Table 2 shows the interobserver agreement among the 3 observers for the 4 imaging modes based on weighted kappa statistics. As shown, the interobserver agreement was higher for objects positioned centrally in the FOV than for those that were positioned peripherally.

The sensitivity, specificity, PPV, NPV, LR+ and LR− for different modes with respect to the position of the object in the FOV were calculated for the 3 observers and are shown in Table 3.

The maximum sensitivity for the first observer was found for objects positioned peripherally in the FOV without use of the MAR algorithm. The maximum sensitivity for the second observer was found for objects positioned peripherally in the FOV when the MAR algorithm was applied. The maximum sensitivity for the third observer was observed for objects positioned centrally in the FOV with or without use of the MAR algorithm. In general, the highest sensitivity was shown by the first observer (66.7%). Only the second observer showed an increase in sensitivity with both peripheral and central positioning of the object in the FOV following application of the MAR algorithm. In general, the second and third observers had better sensitivity for objects positioned centrally in the FOV, irrespective of the effect of the MAR algorithm.

In general, and for all observers, accuracy was higher for objects positioned centrally within the FOV than for objects positioned peripherally, with or without application of the MAR algorithm.

Specificity values were generally high for all modes and all observers, indicating a high percentage of correct detection of sound teeth (without VRFs) in all 4 modes.

Table 4 and Table 5 present the sensitivity, specificity, PPV, NPV, LR+, and LR− for different imaging modes for the 3 observers according to the position of the object in the FOV, the presence or absence of metal casting posts, and whether the MAR algorithm was applied. The presence of metal casting posts significantly decreased the sensitivity, specificity, PPV, and NPV. However, the first observer showed the highest sensitivity for objects positioned peripherally in the FOV without activating the MAR algorithm in the absence of casting posts.

In the presence of casting posts, the highest sensitivity was observed for objects positioned centrally in the FOV without applying the MAR algorithm. The second observ-

Table 3. Sensitivity, specificity, positive predictive value (PPV), negative predictive value (NPV), positive likelihood ratio (LR+), and negative likelihood ratio (LR–) for different imaging modes according to the position of the object in the field of view and application of the metal artifact reduction algorithm for the 3 observers

	Peripheral + no MAR			Peripheral + MAR			Central + no MAR			Central + MAR		
	Observer 1	Observer 2	Observer 3	Observer 1	Observer 2	Observer 3	Observer 1	Observer 2	Observer 3	Observer 1	Observer 2	Observer 3
Sensitivity (CI)	66.7 (54.7-78.6)	23.3 (12.6-34)	53.3 (40.7-66)	53.3 (40.7-66)	46.7 (34-59.2)	53.3 (40.7-66)	63.3 (51.1-75.5)	50 (37.4-62.7)	60 (47.6-72.4)	63.3 (51.1-75.5)	63.3 (51.14-75.53)	60 (47.6-72.4)
Specificity (CI)	76.7 (66-87.3)	90 (82.4-98)	60 (47.6-72.4)	73.3 (62.1-84.5)	70 (58.4-81.6)	83.3 (73.9-92.8)	83.3 (73.9-92.8)	73.3 (62.1-84.5)	60 (47.6-72.4)	76.7 (66-87.4)	63.3 (51.1-75.5)	83.3 (73.9-92.8)
Accuracy	71.7	56.7	56.7	63.3	58.3	68.3	73.3	61.7	60.0	70.0	63.3	71.7
PPV (CI)	74.1 (63-85.2)	70 (58.4-81.6)	57.1 (44.6-69.7)	66.7 (54.7-78.6)	60.9 (48.5-73.2)	76.2 (65.4-87)	79.2 (68.9-89.4)	65.2 (53.2-77.3)	60 (47.6-72.4)	73.1 (61.9-84.3)	63.3 (51.1-75.5)	78.3 (67.8-88.7)
NPV (CI)	69.7 (58.1-81.3)	54 (41.4-66.6)	56.2 (43.7-68.8)	61.1 (48.8-73.5)	56.8 (44.2-69.3)	64.1 (52-76.2)	69.4 (57.8-81.1)	59.5 (47-71.9)	60 (47.6-72.4)	67.7 (55.8-79.5)	63.3 (51.1-75.5)	67.6 (55.7-79.4)
LR+ (CI)	2.8 (1.4-5.7)	2.3 (0.7-8.2)	1.3 (0.8-2.3)	2 (1.1-4)	1.6 (0.8-3.3)	3.2 (1.3-7.6)	3.8 (1.6-8.8)	1.9 (0.9-3.7)	1.5 (0.9-2.5)	2.7 (1.3-5.5)	1.7 (1-3)	3.6 (1.5-8.4)
LR– (CI)	0.4 (0.3-0.7)	0.9 (0.7-1.1)	0.8 (0.5-1.3)	0.6 (0.4-1.0)	0.8 (0.5-1.1)	0.6 (0.4-0.9)	0.4 (0.3-0.7)	0.7 (0.4-1.0)	0.7 (0.4-1.1)	0.5 (0.3-0.8)	0.6 (0.3-1)	0.5 (0.3-0.8)

MAR: metal artifact reduction

Table 4. Sensitivity, specificity, positive predictive value (PPV), negative predictive value (NPV), positive likelihood ratio (LR+), and negative likelihood ratio (LR–) for different imaging modes according to the position of the object in the field of view for the 3 observers in the absence of intracanal posts

	Peripheral + no MAR			Peripheral + MAR			Central + no MAR			Central + MAR		
	Observer 1	Observer 2	Observer 3	Observer 1	Observer 2	Observer 3	Observer 1	Observer 2	Observer 3	Observer 1	Observer 2	Observer 3
Sensitivity (CI)	86.6 (74.5-98.8)	20 (5.7-34.3)	66.6 (49.8-83.5)	73.3 (57.5-89.1)	66.7 (49.8-83.5)	66.7 (49.8-83.5)	66.7 (49.8-83.5)	46.7 (28.8-64.5)	60 (42.5-77.5)	73.3 (57.5-89.2)	66.6 (49.8-83.5)	73.3 (57.5-89.2)
Specificity (CI)	93.3 (84.4-102.2)	93.3 (84.4-102)	60 (42.5-77.5)	80 (65.6-94.3)	80 (65.6-94.3)	80 (65.6-94.3)	93.3 (84.4-102)	93.3 (84.4-102)	60 (42.5-77.5)	86.7 (74.5-98.8)	80 (65.6-94.3)	86.6 (74.5-98.8)
Accuracy	90	56.7	63.3	76.7	73.4	73.4	80	70	60	80	73.3	80
PPV (CI)	92.8 (83.6-102.7)	75 (59.5-90.5)	63 (45.2-79.8)	79 (63.8-93.2)	77 (61.8-92)	77 (61.8-92)	91 (80.6-101)	88 (75.7-99.3)	60 (42.5-77.5)	84.6 (71.7-97.5)	76.9 (61.8-92)	84.6 (71.7-97.5)
NPV % (CI)	87.5 (75.6-99.3)	53.8 (36-71.7)	64.3 (47.1-81.4)	75 (59.5-90.4)	70.5 (54.3-86.9)	70.5 (54.2-86.8)	73.7 (57.9-89.4)	63.4 (46.4-80.8)	60 (42.5-77.5)	76.4 (61.3-91.6)	70.5 (54.2-86.8)	76.4 (61.3-91.6)
LR+ (CI)	13 (1.9-87.3)	3.0 (0.4-25.7)	1.7 (0.8-3.4)	3.7 (1.3-10.6)	3.3 (1.1-9.8)	3.3 (1.1-9.8)	10 (1.5-68.7)	7 (1-50.2)	1.5 (0.7-3.2)	7.4 (2-27.4)	3.6 (1.2-10.5)	5.5 (1.5-20.7)
LR– (CI)	0.1 (0.1-0.5)	0.9 (0.6-1.1)	0.6 (0.2-1.3)	0.3 (0.1-0.8)	0.4 (0.2-0.9)	0.4 (0.2-0.9)	0.4 (0.2-0.7)	0.6 (0.3-0.9)	0.7 (0.3-1.4)	0.1 (0.1-0.5)	0.4 (0.2-0.9)	0.3 (0.1-0.7)

MAR: metal artifact reduction

Table 5. Sensitivity, specificity, positive predictive value (PPV), negative predictive value (NPV), positive likelihood ratio (LR+), and negative likelihood ratio (LR−) for different imaging modes according to the position of the object in the field of view for the 3 observers in the presence of an intracanal post

	Peripheral + no MAR			Peripheral + MAR			Central + no MAR			Central + MAR		
	Observer 1	Observer 2	Observer 3	Observer 1	Observer 2	Observer 3	Observer 1	Observer 2	Observer 3	Observer 1	Observer 2	Observer 3
Sensitivity (CI)	46.7 (28.8-64.5)	26.6 (10.8-42.5)	40 (22.5-57.5)	33.3 (16.4-50.2)	26.6 (10.8-42.5)	40 (22.5-57.5)	60.00 (42.5-77.5)	53.30 (35.4-71.2)	60.00 (42.5-77.5)	53.3 (35.4-71.2)	60 (42.5-77.5)	46.7 (28.8-64.5)
Specificity (CI)	60 (42.5-77.5)	86.6 (74.5-98.8)	60 (42.5-77.5)	66.6 (49.8-83.5)	60 (42.5-77.5)	86.6 (74.5-98.8)	73.3 (57.5-89.2)	53.3 (35.4-71.2)	60 (42.5-77.5)	66.6 (49.8-83.5)	46.7 (28.8-64.5)	80 (65.7-94.3)
Accuracy	53.35	56.6	50	50	43.3	63.3	66.7	53.3	60	60	53.4	63.3
PPV (CI)	53.8 (36-71.7)	66.6 (49.8-83.5)	50 (32.1-67.8)	50 (32.1-67.8)	40 (22.4-57.5)	75 (59.5-90.5)	69.2 (52.7-85.7)	53.3 (35.4-71.2)	60 (42.5-77.5)	62 (44.1-78.9)	53 (35.1-70.8)	70 (53.6-86.4)
NPV (CI)	52.9 (35.1-70.8)	54.20 (36.3-72)	50.00 (32.1-67.8)	50.00 (32.1-67.8)	45.00 (27.2-62.8)	59.10 (41.5-76.7)	64.70 (47.6-81.8)	53.30 (35.4-71.2)	60.00 (42.5-77.5)	58.80 (41.2-76.4)	53.80 (36.1-71.7)	60 (42.5-77.5)
LR+ (CI)	1.2 (0.5-2.7)	2.0 (0.4-9.3)	1.0 (0.4-2.4)	1.0 (0.4-2.8)	0.7 (0.2-1.8)	3.0 (0.7-12.6)	2.3 (0.9-5.7)	1.1 (0.6-2.3)	1.5 (0.7-3.2)	1.6 (0.7-3.7)	1.1 (0.6-2.1)	2.3 (0.7-7.4)
LR− (CI)	0.9 (0.5-1.7)	0.8 (0.6-1.2)	1.0 (0.6-1.8)	1.0 (0.6-1.7)	1.2 (0.7-2.1)	0.7 (0.4-1.1)	0.5 (0.3-1.1)	0.9 (0.4-1.8)	0.7 (0.3-1.4)	0.7 (0.4-1.3)	0.85 (0.4-2)	0.7 (0.4-1.1)

MAR: metal artifact reduction

er showed the highest sensitivity for the detection of VRFs in teeth without casting posts positioned peripherally or centrally in the FOV following application of the MAR algorithm. In the presence of posts, the highest sensitivity was found for objects positioned centrally in the FOV following activation of the MAR algorithm.

In the absence of posts, the third observer showed the highest sensitivity for the detection of VRFs in teeth positioned at the center of the FOV following activation of the MAR algorithm. In the presence of posts, the third observer showed the highest sensitivity for the detection of VRFs in teeth positioned at the center of the FOV without using the MAR algorithm. In general, in the presence of intracanal posts, central positioning of the object in the FOV significantly increased the diagnostic sensitivity and accuracy of the observers compared to the peripheral position with or without activation of the MAR algorithm. The same was not true for all observers in the absence of intracanal posts.

Discussion

Metal artifacts are among the most important factors that affect the diagnostic quality of CBCT images.[18] The high-density materials used for root canal fillings can create artifacts that complicate the detection of VRFs.[19-21] Therefore, this study evaluated the effects of factors such as object position in the FOV, application of the MAR algorithm, the presence or absence of a metal post, and the observer's experience and expertise on the diagnostic sensitivity and accuracy of CBCT images for the detection of VRFs.

Many studies have evaluated the effect of MAR algorithms on the diagnostic accuracy of CBCT images and have yielded controversial results. Bezerra et al.[17] evaluated the effect of the artifact reduction (AR) algorithm in the Picasso Trio 3D CBCT system on the detection of VRFs in teeth with casting posts. Five experienced oral and maxillofacial radiologists with at least 4 years of clinical experience evaluated images of the apical, middle, and cervical thirds of the roots and concluded that in general, application of the AR algorithm decreased the amount of artifacts but negatively affected the diagnostic accuracy for VRF detection. Contrary to their expectations, the AR algorithm did not improve the detection of VRFs in the presence of intracanal posts.

Bechara et al.[22] compared the ProMax (Planmeca, Helsinki, Finland) and Master 3D (Vatech, Hwaseong, Republic of Korea) CBCT systems for the detection of root fracture lines in endodontically treated teeth with or without application of the AR algorithm. The sensitivity of both

CBCT systems was higher when the AR algorithm was not applied, and the sensitivity and specificity of the ProMax CBCT system were higher than those of the Master 3D system. Use of the AR algorithm in both systems decreased the diagnostic accuracy for detection of root fractures. In general, application of the AR algorithm improves image quality, but negatively affects the diagnostic value for detection of VRFs.

Dalili Kajan et al.[23] evaluated the efficacy of application of the MAR algorithm for the detection of root fractures in the absence and presence of intracanal posts on CBCT images. The highest frequency of root fracture diagnoses occurred in the MAR mode when the post space remained empty. Furthermore, application of the MAR mode in both the pin and post space groups increased the diagnostic accuracy, although this difference did not reach statistical significance. Moreover, the sensitivity of the MAR mode was higher than without the MAR mode in both the pin and post space groups.

The current study showed that application of the MAR algorithm had no significant negative effect on the frequency of correct diagnoses of VRFs and diagnostic sensitivity, except for the first observer with peripheral positioning of the object in the FOV, and either confirmed or improved the accuracy of diagnosis. However, only the second observer showed a significant difference in the frequency of correct diagnoses with different positions of the object in the FOV and depending on the application of the MAR algorithm. Activation of the MAR algorithm for the second observer increased the frequency of correct diagnoses of VRFs and diagnostic sensitivity in both central and peripheral positions of the object in the FOV. In other words, only the results for our first observer were in line with the findings of the aforementioned studies,[17,22] and the results for the remaining 2 observers were in agreement with those of Dalili Kajan et al.[23] The diagnostic accuracy in these 2 observers improved to some extent, in accordance with the findings of Dalili Kajan et al.[23] Activation of the MAR algorithm slightly decreased the diagnostic accuracy for the detection of VRFs by the first observer, who was an experienced oral and maxillofacial radiologist expert on the detection of root fractures. The results of our first observer were in accord with those of Bezerra et al.[17] and Bechara et al.[22]

Object position in the FOV is another influential factor on the diagnostic quality of CBCT images. In 2017, Queiroz et al.[15] assessed the efficacy of the MAR tool for noise reduction with different positions of the object in the FOV (peripheral and central). They found a higher level of noise on the images of phantoms positioned peripherally in the FOV when the MAR tool was disabled. However, in contrast to their expectations, activating the MAR tool increased the level of noise when the phantom was positioned in the periphery of the FOV. A reduction in noise following activation of the MAR tool only occurred when the phantom was placed at the center of the FOV. In general, following activation of the MAR tool, the greatest difference in the level of noise was found when comparing the peripheral and central positions of objects in the FOV; with peripheral positioning of the metal object in the FOV, activation of the MAR tool increased the noise. They found that the MAR tool had the highest efficacy for metal objects centrally positioned in the FOV. Moreover, image noise was significantly reduced following activation of the MAR tool.[15] Iikubo et al.[24] concluded that small voxel size and a central position of the object in the FOV in CBCT reduced induced metal artifacts. In the current study, the sensitivity, specificity, and diagnostic accuracy increased for objects centrally positioned in the FOV in the presence of intracanal metal posts and following application of the MAR algorithm, which is in agreement with the results of Quiroz et al.[15] and Iikubo et al.[24] However, in teeth with empty post space or gutta-percha in the root canal, activation of the MAR algorithm caused no difference in sensitivity for objects positioned centrally or peripherally in the FOV. In another study, Queiroz et al.[25] evaluated the effect of the MAR algorithm on CBCT images of different dental materials and concluded that the MAR algorithm was ineffective in the presence of gutta-percha. Their explanation for this finding was that gutta-percha does not generate many artifacts that can be significantly decreased by the MAR algorithm, which was in accordance with the results of our study.

Pauwels et al.[14] evaluated the role of the size of the FOV and object position in the reduction of beam scattering and noise on CBCT images. They demonstrated that central positioning of the phantom in the FOV resulted in a reduction in the signal difference to noise ratio (SDNR) following an increase in FOV size. Furthermore, central positioning of the phantom in the FOV decreased the SDNR.

In this study, the position of the object in the FOV had a greater effect than application of the MAR algorithm on diagnostic sensitivity and accuracy, with all 3 observers showing higher diagnostic sensitivity and accuracy with the object in the central position in the FOV (compared to the peripheral position), especially in the presence of metal posts. Only the first observer showed the highest diagnostic accuracy for the detection of VRFs in teeth without

metal posts positioned peripherally in the FOV without application of the MAR algorithm (peripheral FOV + no MAR). Our first observer was an experienced oral and maxillofacial radiologist with longer paraclinical experience in detecting VRFs. Since she often evaluates images in clinical practice without the MAR algorithm with structures of interest in the peripheral FOV, her eyes are probably accustomed to detecting artifacts in this mode. However, the remaining 2 observers showed higher diagnostic sensitivity and accuracy for the detection of VRFs when objects were centrally positioned in the FOV in the presence and absence of metal posts. The third observer was an endodontist who was familiar with the relevant clinical aspects, in addition to the CBCT findings of VRFs, based on his clinical experience. Thus, the third observer was more successful than the second one (an oral and maxillofacial radiologist with 6 years of experience) in the evaluation of CBCT images.

Salineiro et al.[26] performed a meta-analysis on root fractures and concluded that the experience and expertise of the observers could significantly affect the results. They considered the possibility of the selection bias by observers on these kinds of studies. Their study revealed that true positive results for maxillofacial radiologists were higher than for endodontists. The level of inconsistency for maxillofacial radiologists was reported to be lower than for endodontists.

The findings of the current study indicate that although factors such as object position in the FOV[3,7,27-29] and application of the MAR algorithm[16,17,22] might increase the diagnostic sensitivity and accuracy of CBCT images for the detection of VRFs, the experience of the clinician and radiologist can moderate the magnitude of the effects of the aforementioned parameters on the results.

In conclusion, a comparison of the results in the presence and absence of intracanal metal posts revealed that all observers had higher diagnostic sensitivity and accuracy in the absence of posts, and this was more significant when the object was positioned peripherally in the FOV than when it was positioned centrally.

In the absence of posts and with peripheral positioning of the object in the FOV, application of the MAR algorithm only increased the diagnostic sensitivity and accuracy of the second observer, while the same condition with central positioning of the object in the FOV increased the diagnostic sensitivity and accuracy of all observers. The variability in the sensitivity and accuracy of the observers was high when the object was positioned peripherally in the FOV and the MAR algorithm was disabled.

In the presence of metal posts and with peripheral positioning of the object in the FOV, application of the MAR algorithm had no significant effect on sensitivity (except for the first observer), while specificity improved (except for the second observer). Furthermore, with central positioning of the object in the FOV, application of the MAR algorithm only had a significant effect on the second observer.

In the presence of metal posts and without application of the MAR algorithm, sensitivity and accuracy were generally higher with central positioning than with peripheral positioning, and this effect was more significant with central positioning of the object and application of the MAR algorithm (compared to peripheral positioning).

The clinical and paraclinical experience of the observers might serve as a confounder, and the MAR algorithm may be less helpful for experienced observers.

Acknowledgements

We would like to thank Dr. Zahra Atrkar Roshan (Department of Biostatistics, Guilan University of Medical Sciences, Rasht, Iran) for her help in analysis of the data.

References

1. Kamburoğlu K, Murat S, Yüksel SP, Cebeci AR, Horasan S. Detection of vertical root fracture using cone-beam computerized tomography: an in vitro assessment. Oral Surg Oral Med Oral Pathol Oral Radiol Endod 2010; 109: e74-81.
2. Tamse A. Vertical root fractures in endodontically treated teeth: diagnostic signs and clinical management. Endod Topics 2006; 13: 84-94.
3. Khedmat S, Rouhi N, Drage N, Shokouhinejad N, Nekoofar MH. Evaluation of three imaging techniques for the detection of vertical root fractures in the absence and presence of gutta-percha root fillings. Int Endod J 2012; 45: 1004-9.
4. Patel S, Dawood A, Ford TP, Whaites E. The potential applications of cone beam computed tomography in the management of endodontic problems. Int Endod J 2007; 40: 818-30.
5. Pauwels R, Stamatakis H, Bosmans H, Bogaerts R, Jacobs R, Horner K, et al. Quantification of metal artifacts on cone beam computed tomography images. Clin Oral Implants Res 2013; 24 Suppl A100: 94-9.
6. Bernardes RA, de Moraes IG, Húngaro Duarte MA, Azevedo BC, de Azevedo JR, Bramante CM. Use of cone-beam volumetric tomography in the diagnosis of root fractures. Oral Surg Oral Med Oral Pathol Oral Radiol Endod 2009; 108: 270-7.
7. Ferreira RI, Bahrami G, Isidor F, Wenzel A, Haiter-Neto F, Groppo FC. Detection of vertical root fractures by cone-beam computerized tomography in endodontically treated teeth with fiber-resin and titanium posts: an in vitro study. Oral Surg Oral Med Oral Pathol Oral Radiol 2013; 115: e49-57.
8. Youssefzadeh S, Gahleitner A, Dorffner R, Bernhart T, Kain-

berger FM. Dental vertical root fractures: value of CT in detection. Radiology 1999; 210: 545-9.
9. Moudi E, Haghanifar S, Madani Z, Alhavaz A, Bijani A, Bagheri M. Assessment of vertical root fracture using cone-beam computed tomography. Imaging Sci Dent 2014; 44: 37-41.
10. Kajan ZD, Taromsari M. Value of cone beam CT in detection of dental root fractures. Dentomaxillofac Radiol 2012; 41: 3-10.
11. Wang P, Yan XB, Lui DG, Zhang WL, Zhang Y, Ma XC. Detection of dental root fractures by using cone-beam computed tomography. Dentomaxillofac Radiol 2011; 40: 290-8.
12. Bornstein MM, Wölner-Hanssen AB, Sendi P, von Arx T. Comparison of intraoral radiography and limited cone beam computed tomography for the assessment of root-fractured permanent teeth. Dent Traumatol 2009; 25: 571-7.
13. Parsa A, Ibrahim N, Hassan B, Syriopoulos K, van der Stelt P. Assessment of metal artefact reduction around dental titanium implants in cone beam CT. Dentomaxillofac Radiol 2014; 43: 20140019.
14. Pauwels R, Jacobs R, Bogaerts R, Bosmans H, Panmekiate S. Reduction of scatter-induced image noise in cone beam computed tomography: effect of field of view size and position. Oral Surg Oral Med Oral Pathol Oral Radiol 2016; 121: 188-95.
15. Queiroz PM, Santaella GM, da Paz TD, Freitas DQ. Evaluation of a metal artefact reduction tool on different positions of a metal object in the FOV. Dentomaxillofac Radiol 2017; 46: 20160366.
16. Bechara BB, Moore WS, McMahan CA, Noujeim M. Metal artefact reduction with cone beam CT: an in vitro study. Dentomaxillofac Radiol 2012; 41: 248-53.
17. Bezerra IS, Neves FS, Vasconcelos TV, Ambrosano GM, Freitas DQ. Influence of the artefact reduction algorithm of Picasso Trio CBCT system on the diagnosis of vertical root fractures in teeth with metal posts. Dentomaxillofac Radiol 2015; 44: 20140428.
18. Barrett JF, Keat N. Artifacts in CT: recognition and avoidance. Radiographics 2004; 24: 1679-91.
19. Özer SY. Detection of vertical root fractures of different thicknesses in endodontically enlarged teeth by cone beam computed tomography versus digital radiography. J Endod 2010; 36: 1245-9.
20. Junqueira RB, Verner FS, Campos CN, Devito KL, do Carmo AM. Detection of vertical root fractures in the presence of intracanal metallic post: a comparison between periapical radiography and cone-beam computed tomography. J Endod 2013; 39: 1620-4.
21. Melo SL, Haiter-Neto F, Correa LR, Scarfe WC, Farman AG. Comparative diagnostic yield of cone beam CT reconstruction using various software programs on the detection of vertical root fractures. Dentomaxillofac Radiol 2013; 42: 20120459.
22. Bechara B, Alex McMahan C, Moore WS, Noujeim M, Teixeira FB, Geha H. Cone beam CT scans with and without artefact reduction in root fracture detection of endodontically treated teeth. Dentomaxillofac Radiol 2013; 42: 20120245.
23. Dalili Kajan Z, Taramsari M, Khosravi Fard N, Khaksari F, Moghasem Hamidi F. The efficacy of metal artifact reduction mode in cone-beam computed tomography images on diagnostic accuracy of root fractures in teeth with intracanal posts. Iran Endod J 2018; 13: 47-53.
24. Iikubo M, Nishioka T, Okura S, Kobayashi K, Sano T, Katsumata A, et al. Influence of voxel size and scan field of view on fracture-like artifacts from gutta-percha obturated endodontically treated teeth on cone-beam computed tomography images. Oral Surg Oral Med Oral Pathol Oral Radiol 2016; 122: 631-7.
25. Queiroz PM, Oliveira ML, Groppo FC, Haiter-Neto F, Freitas DQ. Evaluation of metal artefact reduction in cone-beam computed tomography images of different dental materials. Clin Oral Investig 2018; 22: 419-23.
26. Salineiro FCS, Kobayashi-Velasco S, Braga MM, Cavalcanti MGP. Radiographic diagnosis of root fractures: a systematic review, meta-analyses and sources of heterogeneity. Dentomaxillofac Radiol 2017; 46: 20170400.
27. Katsumata A, Hirukawa A, Okumura S, Naitoh M, Fujishita M, Ariji E, et al. Relationship between density variability and imaging volume size in cone-beam computerized tomographic scanning of the maxillofacial region: an in vitro study. Oral Surg Oral Med Oral Pathol Oral Radiol Endod 2009; 107: 420-5.
28. van Daatselaar AN, Dunn SM, Spoelder HJ, Germans DM, Renambot L, Bal HE, et al. Feasibility of local CT of dental tissues. Dentomaxillofac Radiol 2003; 32: 173-80.
29. Katsumata A, Hirukawa A, Okumura S, Naitoh M, Fujishita M, Ariji E, et al. Effects of image artifacts on gray-value density in limited-volume cone-beam computerized tomography. Oral Surg Oral Med Oral Pathol Oral Radiol Endod 2007; 104: 829-36.